Direct Adaptive Current Control
A universal current control scheme for electrical machines

Andreas Liske, Michael Braun
Karlsruhe Institute of Technology (KIT)
Elektrotechnisches Institut (ETI) - Electrical Drives and Power Electronics
Kaiserstr. 12, 76131 Karlsruhe, Germany
Phone: +49 (0) 721-608-46848
Andreas.Liske@kit.edu, www.eti.kit.edu

***Abstract*—This paper presents a direct, adaptive and parameter-free current control scheme that is independent of the motor type and doesn't need any machine parameters. A given setpoint can be reached accurately within one switching cycle.**

I. Introduction

In recent years many advanced current control strategies for electrical machines have been investigated and published. Most of them can be classified into linear, hysteresis, sliding mode, fuzzy and predictive control. In [1] the field of predictive control is further broken down into hysteresis based, trajectory based, dead beat and model predictive control. Especially model predictive control (MPC) [2] offers great possibilities since even complex physical side-effects that are often neglected can be controlled. This is done by online calculation of a detailed model, that includes for example saturation effects [3] or even cross-coupling effects [4] of permanent magnet synchronous machines. The drawbacks of many predictive control schemes on the other hand are versatile and often combined. One of them is the dependency on machine parameters that may vary during operation, leading to a suboptimal and sometimes fragile control setup. Another is the use of complex mathematical machine models, which increases the required computing time. If hysteresis controllers are used, the varying switching frequency makes appropriate filter design a complex task. Notably, MPC and the field of sensorless control [5] has been investigated exhaustively, so that meanwhile there are improvements and advanced control strategies available, that have overcome the drawbacks for some of those control schemes [6], [7].

In [8]–[10] the "Straightforward Current Control" (SCC) scheme has been presented for the control of a DC machine as well as for the control of magnetic isotropic 3-phase synchronous machines (with $L_d = L_q$), that delivers excellent control quality and high dynamics. At the same time it doesn't need any machine parameters, no machine model, no test pulses, no offline calculations or cost functions and the computational effort is comparatively little. The system is identified permanently in every pulse period by measuring the slopes of the stator currents in each of the applied switching states, making the SCC completely adaptive. It could be classified as a model-free dead-beat control scheme. One main limitation of this standard SCC control scheme is that it is only suited for magnetic isotropic machines with $L_d = L_q$. When it is applied to a magnetic anisotropic machine with $L_d \neq L_q$, the control quality significantly decreases with a growing magnetic anisotropy.

A solution to solve this limitation was presented in [11] with a new algorithm called "Extended Straightforward Current Control" (ESCC). This algorithm additionally allows to control the currents of synchronous machines with magnetic anisotropic characteristics, such as interior permanent magnet synchronous machines (IPMSM), as well as magnetic isotropic machines without changes in the algorithm itself.

So far the ESCC was introduced as a current control algorithm for synchronous machines only. This paper shows that the same control algorithm is also suited to control the currents of induction motors as well. Again, no changes in the control algorithm are necessary. With this additional capability this control scheme becomes an universal, parameter-free, adaptive current control scheme for three phase machines. To emphasize this universal usability and it's direct control character, the ESCC is renamed and further referred to as "Direct Adaptive Current Control" (DACC).

After a short introduction to the working principle of this control scheme, the theory for the different machine types is developed. Then the algorithm presented in [11] is outlined to show why it can handle all machine types without changes and the need for setup-parameters. Concluding this paper, simulation results are shown.

II. Basic working principle

The basic working principle of the DACC control scheme is best explained with a one-phase RL-load as depicted in Figure 1. By operating the switch with the duty cycle $a = T_{ON}/T_P$, the voltage u_{DC} is applied to the RL-load. Given that the

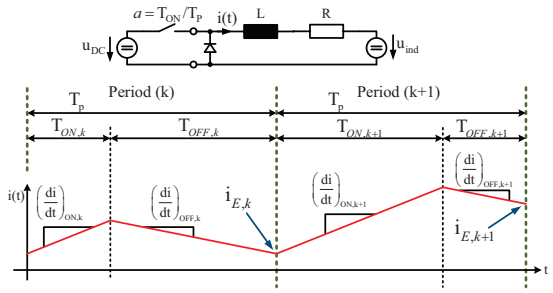

Figure 1. Basic working principle of the DACC, illustrated with a one-phase RL-load

switching frequency is high enough, the current will rise and fall linear in straight line segments. The current slopes for each switching state of period k $(\mathrm{di}/\mathrm{dt})_{\mathrm{ON,k}}$ and $(\mathrm{di}/\mathrm{dt})_{\mathrm{OFF,k}}$ can be assumed to be the same in period k+1 if the applied voltage, the inductance and the resistance are approximately constant for two consecutive periods. This usually is given due to the relatively high switching frequency. Once the current slopes of period k are known for every switching state, the necessary duty cycle for a given current setpoint $i_{E,k+1}$ that should be reached at the end of the next period k+1 can be calculated easily with a linear equation. The knowledge of the absolute voltage, the inductance and the resistance is not needed. The current slopes are detected in every period, which means that this control strategy is completely adaptive.

For three phase applications the very same principle can be applied as shown in [9]. The basis for the DACC [11] and the preceding control schemes [8]–[10] is the fast detection of the stator current slopes during each switching state S_n with $n \in \{1..8\}$ of the utilized voltage source inverter (VSI). This can be done by measuring the stator currents during each switching state in every period very fast with oversampling of the A/D-converter. The calculation of the current slopes then is done with a least-squares-estimator-algorithm to eliminate noise at the end of the same period (index k) in an FPGA (see Figure2). Due to the fast calculation possibilities in the FPGA,

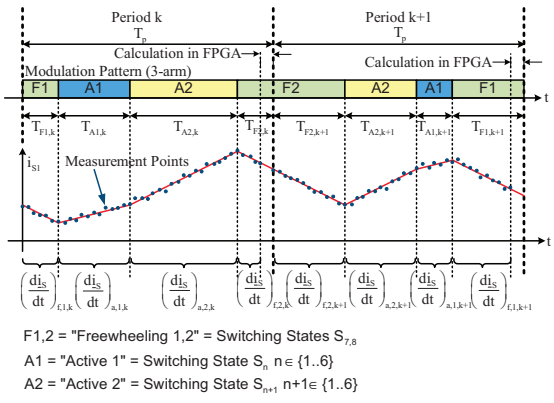

Figure 2. Timing, modulation and measurement principle of the DACC. Although all three stator phase currents are measured, in this diagram only i_{S1} is outlined to improve clarity.

the results can be utilized directly for the calculation of the duty-cycles of the next pulse period k+1, which minimizes control dead-time significantly. The switching frequency is assumed to be high enough so that the current slopes can be considered as being linear during the switching states.

The so gained current slopes $\left(\frac{d\underline{i}_S}{dt}\right)_{a,n,k}$ and $\left(\frac{d\underline{i}_S}{dt}\right)_{f,k}$ are used to define the so called "current gradient vectors" $\Delta\underline{i}_{a,n,k}$ and $\Delta\underline{i}_{f,k}$ [9]:

$$\Delta\underline{i}_{a,n,k} = \left[\left(\frac{\mathrm{d}}{\mathrm{dt}}\underline{i}_S\right)_{a,n,k} - \left(\frac{\mathrm{d}}{\mathrm{dt}}\underline{i}_S\right)_{f,k}\right] \cdot T_p \tag{1}$$

$$\Delta\underline{i}_{f,k} = \left(\frac{\mathrm{d}}{\mathrm{dt}}\underline{i}_S\right)_{f,k} \cdot T_p \tag{2}$$

The index a stands for an active switching state, where the machine is connected to the dc link voltage. Which one of the six possible switching states is applied is denoted with the index n. The index f indicates the freewheeling switching states respectively. The current gradient vectors $\Delta\underline{i}_{a,n,k}$ describe the current variation that would occur, if only the voltage corresponding to the active switching state with the index n would be applied to the machine for the whole period (T_p) with the index k. Similarly $\Delta\underline{i}_{f,k}$ depicts the current variation that would occur, if only a freewheeling switching state would be applied to the machine for the whole pulse period k. In three phase systems they can be represented as current space vectors in the stator-oriented complex $\alpha\beta$-plane [10] (see Figure 4).

This information about the current variation depending on the switching states can be used to calculate the necessary duty cycles for the next period to reach a desired setpoint value directly.

The green vector diagram in Figure 4 depicts the essential of the DACC algorithm: The last value of the stator current at the end of the preceding period is represented by the red current space vector $\underline{i}_{e,k}$. The inner voltage of the machine is effective anyway, so its influence to the current variation $\Delta\underline{i}_{f,k}$ can be added to $\underline{i}_{e,k}$ directly. The resulting vector $\underline{i}_{f,k+1}$ now represents the origin of the hexagons spanned by the current gradient vectors for the active switching states $\underline{i}_{a,n,k}$. Since the control algorithm in the FPGA is started shortly before the end of the current period k, the necessary value $\underline{i}_{e,k}$ for this equation can not be measured, but can be calculated by extrapolation of the just measured current slopes and the knowledge of the applied duty cycles in period k. With $\underline{i}_{f,k+1}$ as starting point, the necessary duty cycles to reach a given current setpoint value $\underline{i}_{e,k+1}$ at the end of period k+1 can be obtained by the projection of the vector $\underline{i}_{a,k+1}$ to the adjacent switching state vectors $\underline{S}_n$.

$$\underline{i}_{a,k+1} = \underline{i}_{e,k+1} - \underline{i}_{f,k+1} = \underline{i}_{e,k+1} - i_{e,k} - \Delta i_{f,k} \tag{3}$$

This is done by using the same computation formulas as with the well known space vector modulation. It is not necessary to know the voltage that is applied to the machine or its inductance and resistance. The only assumption that has to be valid

is, that the current gradient vectors are approximately constant for two consecutive periods, so that $\Delta\underline{i}_{a,n,k} \approx \Delta\underline{i}_{a,n,k+1}$ and $\Delta\underline{i}_{f,k} \approx \Delta\underline{i}_{f,k+1}$ is given.

The DACC algorithm evaluates the measured current gradient vectors and hence is based on the knowledge of the functional dependencies of them. In the following section, the current gradient vectors for the different machine types shown in Figure 4 are derived and compared.

III. Current Gradient Vectors for Different Types of Three Phase Machines

The derivation of the current gradient vectors for synchronous machines has been presented in [11]. It will be outlined here again to be able to compare it directly with the derivation and the results of the current gradient vectors for the induction machines.

A. Synchronous machines

Starting point are the system equations of the synchronous machine, transformed into the stator-oriented $\alpha\beta$-reference frame [12]:

$$\begin{aligned}\underline{u}_S &= R_S\underline{i}_S + \underline{L}_A\frac{d}{dt}\underline{i}_S \\ &+ \frac{d}{dt}\underline{L}_B\cdot\underline{i}_S + \underline{L}_B\cdot\frac{d}{dt}\underline{i}_S + \frac{d}{dt}\underline{\Psi}_{PMS}\end{aligned} \tag{4}$$

with

$$\underline{L}_A = \begin{pmatrix} \frac{3}{2}L_A & 0 \\ 0 & \frac{3}{2}L_A \end{pmatrix} \tag{5}$$

$$\underline{L}_B = \frac{3}{2}L_B\cdot\begin{pmatrix} \cos(2\gamma(t)) & \sin(2\gamma(t)) \\ \sin(2\gamma(t)) & -\cos(2\gamma(t)) \end{pmatrix} \tag{6}$$

$$\mathrm{L}_A = \frac{1}{3}(L_d + L_q) \qquad \mathrm{L}_B = \frac{1}{3}(L_d - L_q) \tag{7}$$

1) Magnetic anisotropic synchronous machines: Equation (4) can be rewritten as a space vector, consisting of the two components $u_{S,\alpha}$ and $u_{S,\beta}$:

$$\begin{aligned}\underline{u}_S = \begin{pmatrix} u_{S,\alpha} \\ u_{S,\beta} \end{pmatrix} &= R_S\begin{pmatrix} i_{S,\alpha} \\ i_{S,\beta} \end{pmatrix} + \underline{L}_A\begin{pmatrix} \frac{d}{dt}i_{S,\alpha} \\ \frac{d}{dt}i_{S,\beta} \end{pmatrix} \\ &+ \frac{d}{dt}\underline{L}_B\begin{pmatrix} i_{S,\alpha} \\ i_{S,\beta} \end{pmatrix} + \underline{L}_B\begin{pmatrix} \frac{d}{dt}i_{S,\alpha} \\ \frac{d}{dt}i_{S,\beta} \end{pmatrix} + \frac{d}{dt}\underline{\Psi}_{PMS}\end{aligned} \tag{8}$$

The equations of $u_{S,\alpha}$ and $u_{S,\beta}$ are solved for the derivatives of the current vector components $\frac{d}{dt}i_{S,\alpha}$ and $\frac{d}{dt}i_{S,\beta}$. With those, the current gradient vector for the freewheeling switching states $\Delta\underline{i}_f$ can be calculated (see also (2)).

$$\Delta\underline{i}_f = \left.\begin{pmatrix} \frac{d}{dt}i_{S,\alpha} \\ \frac{d}{dt}i_{S,\beta} \end{pmatrix}\right|_{\mathrm{u_{S\alpha}=u_{S\beta}=0}}\cdot T_p = \begin{pmatrix} \Delta i_{f,\alpha} \\ \Delta i_{f,\beta} \end{pmatrix} \tag{9}$$

The current gradient vectors of the six active switching states are (see also (1))

$$\Delta\underline{i}_{a,n} = \begin{pmatrix} \frac{d}{dt}i_{S,\alpha} \\ \frac{d}{dt}i_{S,\beta} \end{pmatrix}\cdot T_p - \Delta\underline{i}_f = \begin{pmatrix} \Delta i_{a,n,\alpha} \\ \Delta i_{a,n,\beta} \end{pmatrix} \tag{10}$$

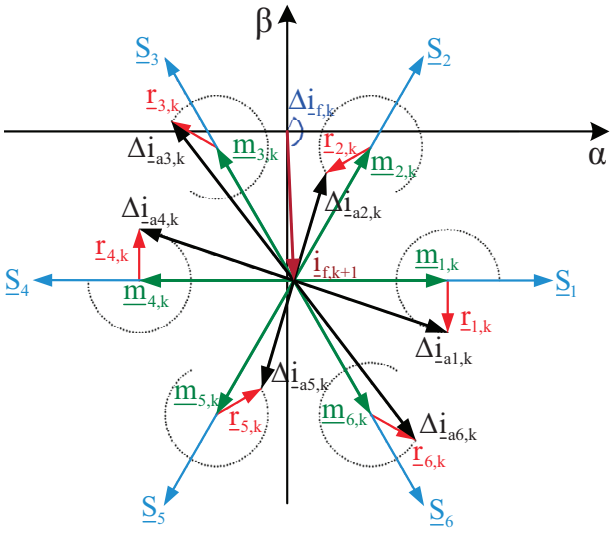

Figure 3. Geometrical locus of $\Delta\underline{i}_{a,n}$ for machines with $L_d \neq L_q$ after a 3/8 electrical period and the vectors $\underline{m}_{n,k}$, $\underline{r}_{n,k}$ and $\Delta\underline{i}_{a,n,k}$ for the current pulse period k.

Solving and rearranging this equation leads to the following mathematical representation:

$$\begin{aligned}\Delta\underline{i}_{a,n} &= \frac{2}{3(L_A^2 - L_B^2)}\cdot u_S\cdot T_p\left(L_A e^{j\varphi_n} - L_B e^{j(2\gamma(t)-\varphi_n)}\right) \\ &= \underbrace{\frac{2u_S T_p}{3(L_A^2 - L_B^2)}L_A e^{j\varphi_n}}_{\underline{m}_n} - \underbrace{\frac{2u_S T_p}{3(L_A^2 - L_B^2)}L_B e^{j(2\gamma(t)-\varphi_n)}}_{\underline{r}_n} \\ &= \underline{m}_n - \underline{r}_n\end{aligned} \tag{11}$$

with

$$\underline{m}_{n,k} = \frac{2u_S T_p}{3(L_A^2 - L_B^2)}\cdot L_A\cdot e^{j\varphi_n} \tag{12}$$

$$\underline{r}_{n,k} = \frac{2u_S T_p}{3(L_A^2 - L_B^2)}\cdot L_B\cdot e^{j[2\gamma_k - \varphi_n]} \tag{13}$$

$$u_S = |\underline{u}_S| = \frac{2}{3}U_{DC} \tag{14}$$

$$\varphi_n = (n-1)\cdot 60° \qquad \mathrm{n} \in \{1..6\} \tag{15}$$

The six current gradient vectors for the current variation during the active switching states can each be represented by two vectors (Fig.3). The constant, time-invariant vectors $\underline{m}_n$ point with the angle φ_n in the direction of the corresponding switching state vectors $\underline{S}_n$. The time-variant vectors $\underline{r}_n$ all have the same constant length and rotate with the doubled angular frequency of the rotor position angle $2\gamma(t)$ around the tip of $\underline{m}_n$, each with an individual angular offset of $-\varphi_n$. Because this angular offset sums up to 180° when looking at two opposite switching states S_n and $S_{n\pm3}$, the current gradient vectors of opposite switching states show a symmetry with respect to the tip of $\underline{i}_{f,k+1}$ (see Fig.4(b) and Fig.3). In Figure 3, the geometrical locus of the six $\Delta\underline{i}_{a,n}$ during a three

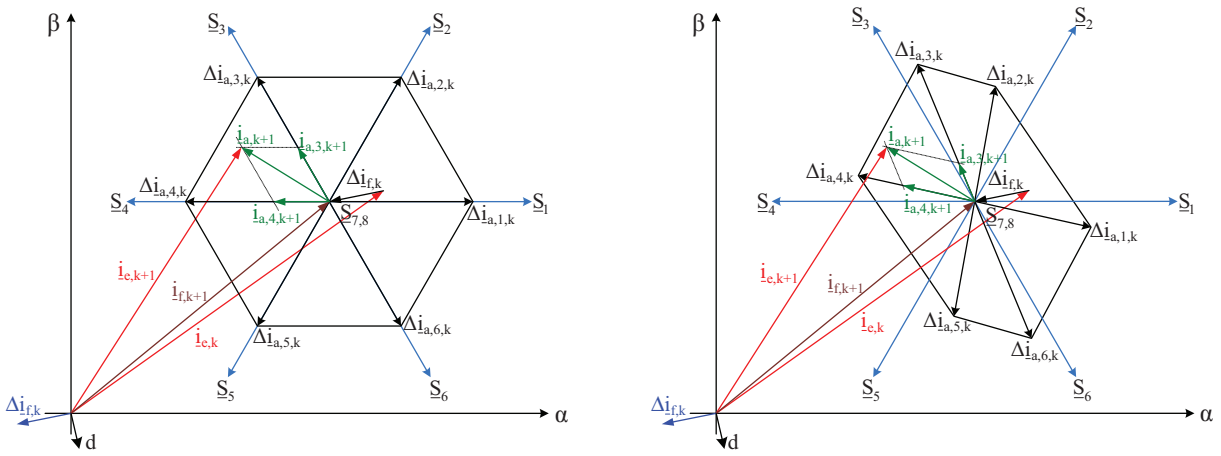

(a) Synchronous machines with $L_d = L_q$ and induction machines

(b) Synchronous machines with $L_d \neq L_q$

Figure 4. Characteristic values $\Delta\underline{i}_{a,n,k}$ and $\Delta\underline{i}_{f,k}$ (black vectors), switching state vectors $\underline{S}_n$ (blue), area of possible current variation in one pulse period k and the vector diagram of the stator current variation during pulse period k+1 for synchronous machines with $L_d = L_q$ and $L_d \neq L_q$

eighth electrical period is displayed. The length of $\underline{r}_n$ and with that the diameter of the black dotted circles directly depends on the difference between L_d and L_q (see also (7)(11)(13))

2) Magnetic isotropic synchronous machines: With $L_d = L_q$, the terms with $(\underline{L}_B)$ are zero, which simplifies equation (4) significantly and leads to the results that are used in the basic SCC scheme as presented in [9], [10], [13]:

All six active current gradient vectors $\Delta\underline{i}_{a,n,k}$ have the same length and the argument is the same as the one of the corresponding switching state vector $\underline{S}_n$ (see Figure 4(a)). So for magnetic isotropic synchronous machines the measurement of only one active switching state is sufficient to know all six active current gradient vectors.

$$\Delta\underline{i}_{a,n,k}\big|_{L_d=L_q} = \Delta I_{a,k} = \frac{2}{3} \cdot \frac{U_{DC,k} T_p}{L_k} \cdot \underline{S}_n \tag{16}$$

$$\underline{S}_n = e^{j\varphi_n} \tag{17}$$

$$\varphi_n = (n-1) \cdot \frac{\pi}{3} \qquad n \in \{1..6\} \tag{18}$$

This spans an equilateral hexagon of the possible current variation, that can be reached within one pulse period, similar to the hexagon known from conventional space vector modulation (see Fig.4(a)). Since the inner voltage of the machine is effective anyway during the whole pulse period, the origin of this hexagon is at the tip of the vector $\underline{i}_{f,k+1}$, which designates the point where the current space vector would be, if no active switching state would be applied during period k+1.

B. Induction machines

The main contribution of this paper is this derivation of the current gradient vectors for induction machines and to show that the DACC algorithm is applicable as an universal control algorithm for both synchronous and induction machines. To get the functional dependency of the current gradient vectors for induction machines, again the system equations now of the induction machine, transformed into the stator-oriented $\alpha\beta$-reference frame [12] is the basis to start with:

$$\begin{aligned} \underline{u}_S &= R_S \cdot \underline{i}_S + \dot{\underline{\Psi}}_S \\ \underline{\Psi}_S &= (L_{Sh} + L_{S\sigma}) \cdot \underline{i}_S + L_{Sh} \cdot \underline{i'}_R \\ \underline{u}_S &= R_S \cdot \underline{i}_S + \frac{d}{dt}\left[(L_{Sh} + L_{S\sigma}) \cdot \underline{i}_S\right] + \frac{d}{dt}\left[L_{Sh} \cdot \underline{i'}_R\right] \end{aligned} \tag{19}$$

With the assumption that the inductances are time-invariant for two consecutive periods, this can be written as:

$$\underline{u}_S = R_S \cdot \underline{i}_S + (L_{Sh} + L_{S\sigma}) \cdot \frac{d}{dt}\underline{i}_S + L_{Sh} \cdot \frac{d}{dt}\underline{i'}_R \tag{20}$$

Solving for the current slopes gives the desired relation:

$$\frac{d}{dt}\underline{i}_S = \frac{1}{(L_{Sh} + L_{S\sigma})}\left(\underline{u}_S - R_S\underline{i}_S - L_{Sh}\frac{d}{dt}\underline{i'}_R\right) \tag{21}$$

With that the current gradient vector $\Delta\underline{i}_{f,k}$ for the freewheeling switching states can directly be calculated ($\underline{u}_S = 0$)

$$\Delta\underline{i}_{f,k} = \left.\frac{d}{dt}\underline{i}_S\right|_{\underline{u}_S=0} = \frac{1}{(L_{Sh} + L_{S\sigma})}\left(-R_S\underline{i}_S - L_{Sh}\frac{d}{dt}\underline{i'}_R\right) \tag{22}$$

The current gradient vectors of the six active switching states are (see also (1))

$$\begin{aligned} \Delta\underline{i}_{a,k} &= \frac{d}{dt}\underline{i}_S - \Delta\underline{i}_{f,k} \\ &= \frac{1}{(L_{Sh} + L_{S\sigma})}\left(\underline{u}_S - R_S\underline{i}_S - L_{Sh}\frac{d}{dt}\underline{i'}_R \right. \\ &\qquad \left. + R_S\underline{i}_S + L_{Sh}\frac{d}{dt}\underline{i'}_R\right) \\ &= \frac{1}{(L_{Sh} + L_{S\sigma})} \cdot \underline{u}_S \end{aligned} \tag{23}$$

L_{Sh} and $L_{S\sigma}$ are scalar and can be assumed to be time-invariant for about two periods. Further there is no dependency

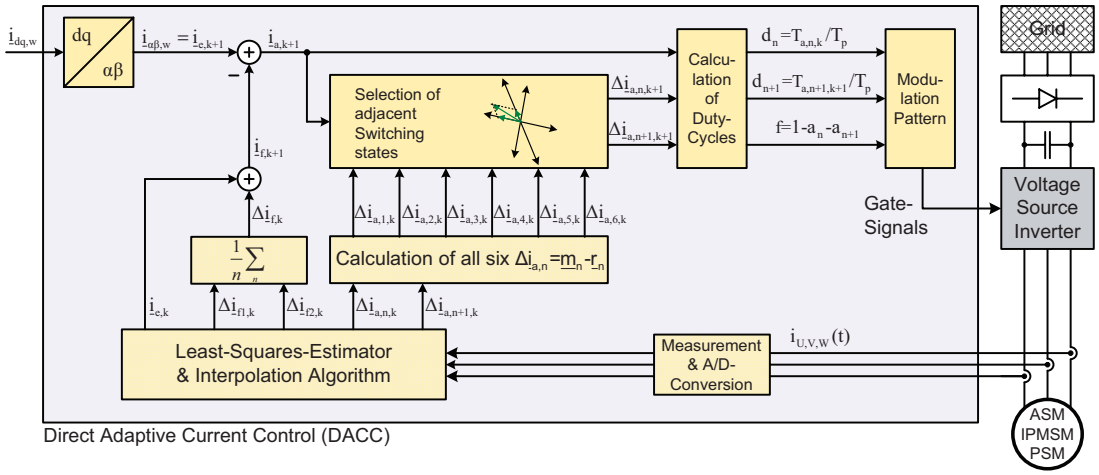

Figure 5. Block diagram of the Direct Adaptive Current Control scheme. The overlaying control, that delivers the required $\underline{i}_{dq,w}$ is not displayed.

on an angle like e.g. with anisotropic synchronous machines. This means that the direction of the $\Delta\underline{i}_{a,k}$ for induction machines only depends on the applied voltage, which is the space vector of one of the six possible active switching states. So for induction machines, all six active current gradient vectors $\Delta\underline{i}_{a,n,k}$ have the same length and the argument is the same as the one of the corresponding switching state vector $\underline{S}_n$. This behavior is similar to magnetic isotropic synchronous machines and the current gradient vectors for induction motors also span an equilateral hexagon (see Fig. 4(a)).

C. Conclusion

The current gradient vectors of induction motors and magnetic isotropic synchronous machines can be seen as special cases of the current gradient vectors of the magnetic anisotropic synchronous machine with the vectors $\underline{r}_{n,k}$ beeing zero. So if the DACC is able to handle the current gradient vectors of magnetic anisotropic synchronous machines it is also capable to control magnetic isotropic synchronous machines and induction machines. And this without the need of telling the control algorithm the type of machine in advance. In the following section, the algorithm of the DACC that was presented in [11] is outlined, to show that it is applicable as an universal current control algorithm for induction and synchronous machines as well.

IV. Direct Adaptive Current Control as Universal Current Control Algorithm

With the analysis of the stator current response to the switching states the DACC scheme can be implemented to realize the vector addition (3) mentioned in II and illustrated in Figure 4.

A. Implementation

1) Least-Squares-Estimator & Interpolation Algorithm: An illustration of the implementation of the DACC is displayed in Figure 5. The currents are measured with a high sampling rate and oversampling during pulse period k, and are input

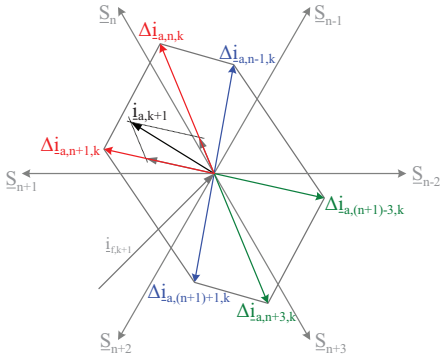

Figure 6. Vector diagram of the algorithm to calculate all six active current gradient vectors.
Red: measured / interpolated
Green: measured values rotated by 180°
Blue: calculated as described in [11]

to the least-squares-estimator algorithm. Here the two current gradient vectors of the switching states that have been applied during period k are calculated. This is $\Delta\underline{i}_{a,n,k}$ for the active switching state vector to the right of $\underline{i}_{a,k}$ (index n), $\Delta\underline{i}_{a,n+1,k}$ for the one to the left of $\underline{i}_{a,k}$ (index n+1) and for the two freewheeling states $\Delta\underline{i}_{f,1,k}$ and $\Delta\underline{i}_{f,2,k}$ (see also Fig.2 and Fig.4(b)). In addition to that, the value of the stator current vector at the end of the current pulse period $\underline{i}_{e,k}$ is calculated by linear extrapolation from the measured current gradient vectors and the knowledge of the applied duty cycles. The current gradient vector $\Delta\underline{i}_{f,k}$ can optionally be calculated as the mean value of the two measured values $\Delta\underline{i}_{f,1,k}$ and $\Delta\underline{i}_{f,2,k}$ to improve accuracy.

In case that the duty cycles are too short to get enough samples in a certain switching state for good accuracy, those current gradient vectors can be calculated by linear interpolation between the values of the adjacent current slopes and the knowledge of the applied duty cycles. This is done directly after the least squares estimator algorithm, so that the

current gradient vectors of both applied active switching states and the freewheeling switching states are known from either measurement or interpolation in every pulse period.

2) Calculation of all six active current gradient vectors: The knowledge of all six current gradient vectors for the active switching states is mandatory for magnetic anisotropic machines, because they permanently vary in length and angle and the plane that is spanned by them is no regular hexagon (see Fig.4(b)). Since only two of the possible six active switching states are applied during one pulse period, only the two current gradient vectors $\Delta\underline{i}_{a,n,k}$ and $\Delta\underline{i}_{a,n+1,k}$ can really be measured, respectively interpolated. In Figure 6 they are displayed as the two red vectors, adjacent to $\underline{i}_{a,k+1}$. The others are calculated, using (11) and the symmetric dependencies coming from this [11]. Opposite current gradient vectors $\Delta\underline{i}_{a,n\pm3,k}$ and $\Delta\underline{i}_{a,(n+1)\pm3,k}$ are derived by simply rotating the corresponding measured current gradient vector by 180°. The two remaining current gradient vectors $\Delta\underline{i}_{a,n-1,k}$ and $\Delta\underline{i}_{a,(n+1)+1,k}$ (blue vectors in Fig.6) can be obtained by solving equation (11). Therefore the two vectors $\underline{m}_{n,k}$ and $\underline{r}_{n,k}$ are necessarily required (see (12)-(15)).

The vectors $\underline{m}_n$ are constant and the angles φ_n are known from their corresponding switching state S_n. The vectors $\underline{r}_{n,k}$ all have the same length and rotate around the tip of the corresponding vector $\underline{m}_{n,k}$, describing circles (3). The length of $\underline{m}_n$ can be obtained by making use of the geometric dependencies of the active current gradient vectors:

The arguments of the six $\underline{r}_{n,k}$ of one pulse period k differ in the angular offset, caused by φ_n. The angle between the vectors $\underline{r}_{n,k}$ and $\underline{r}_{n+1,k}$ of two adjacent switching states is always -60°: In is shown in [11], that by measuring only the two current gradient vectors of the adjacent switching states, all six current gradient vectors can be obtained. That means, that only one pulse period is enough to completely identify the stator current response to all possible switching states and therefore the current control loop system dynamics.

3) Selection of Switching States & Calculation of duty-cycles: In contrary to conventional SVM the segment, and with that the set of two adjacent switching state vectors, can not be changed every 60° anymore because of the time-variant $\Delta i_{a,n,k}$ of magnetic anisotropic synchronous machines. It has to be decided in every single switching cycle, which of the possible six pairs of adjacent active switching states leads to the desired current change $\underline{i}_{a,k+1}$. This can be done by simply calculating the duty-cycles for all six pairs of adjacent active switching states. The pair, where both duty cycles are greater or equal to zero then is to be taken.

For the calculation of the duty-cycles the vector $\underline{i}_{a,k+1}$ is necessary (see Figure 4(b) and 5). It is calculated by vector addition of the setpoint value $\underline{i}_{e,k+1}$ and the vector $\underline{i}_{f,k+1}$:

$$\underline{i}_{a,k+1} = \underline{i}_{e,k+1} - \underline{i}_{f,k+1} = \underline{i}_{e,k+1} - i_{e,k} - \Delta i_{f,k}$$

The calculation of the duty cycles itself is done with the known techniques also applied in conventional SVM. Those duty cycles are input to the space vector modulator, which uses them to output the gate signals according to the implemented pulse pattern.

This algorithm measures the current gradient vectors and uses them to calculate the vector diagram of Figure 4 to get the duty cycles for the next period. This is done with any form of hexagon symmetric with respect to the origin at the tip of vector $\underline{i}_{f,k+1}$. The current gradient vectors are identified permanently from switching cycle to switching cycle. Isotropic synchronous machines and induction machines represent the special case in which the vectors $\underline{r}_{n,k} = 0$ and the irregular hexagon falls back to the regular hexagon marked by the vectors $\underline{m}_n$. This is the reason why the DACC is suitable to control the currents of all of those described machines.

V. Simulation results

The DACC control scheme has been implemented in a Matlab/Simulink-simulation to develop and proof the theory. The simulation parameters have been taken from the hardware test plant, that was used by [10] to proof the basic SCC for synchronous machines with $L_d = L_q$. The main simulation parameters are listed in table I.

Table I
MAIN SIMULATION PARAMETERS

Parameter	anisotropic SM	isotropic SM	Induction M.
DC-link Voltage	$400V$	$400V$	$400V$
Inductance	$L_d = 2\text{mH}$	$L_d = 3\text{mH}$	$L_h = 34,5\text{mH}$
Inductance	$L_q = 4\text{mH}$	$L_q = 3\text{mH}$	$L_s = 0,6\text{mH}$
Pulse Period T_p	$200\mu\text{s}$	$200\mu\text{s}$	$200\mu\text{s}$
Sample Rate T_{AD}	$0.8\mu\text{s}$	$0.8\mu\text{s}$	$0.8\mu\text{s}$

The Figures 7(a),7(b) and 7(c) show the stator currents, controlled by the DACC algorithm in startup and steady state condition. A closer look at startup and a setpoint step of 5A in i_q is displayed in Figure 7(d),7(e) and 7(f). This setpoint step is also shown in the rotor-oriented reference frame with i_d and i_q in Figure 7(g),7(h) and 7(h). The excellent dynamics and steady state accuracy is obvious and shows that the ESCC is well suited to control induction motors as well as isotropic or anisotropic machines without a change in the algorithm.

VI. Conclusion

This paper describes that the DACC scheme presented in [11] is not only capable of controlling synchronous machines, but also covers induction machines as well. There is no need to adjust this control algorithm with machine parameters because it is completely adaptive. The necessary equations are derived from the system equations of the permanent magnet synchronous machine and of the induction machine. The DACC control algorithm is briefly outlined and it is shown how it can control the different machines types without changing the algorithm or the need for machine parameters. The control quality and the dynamics are demonstrated by simulation results.

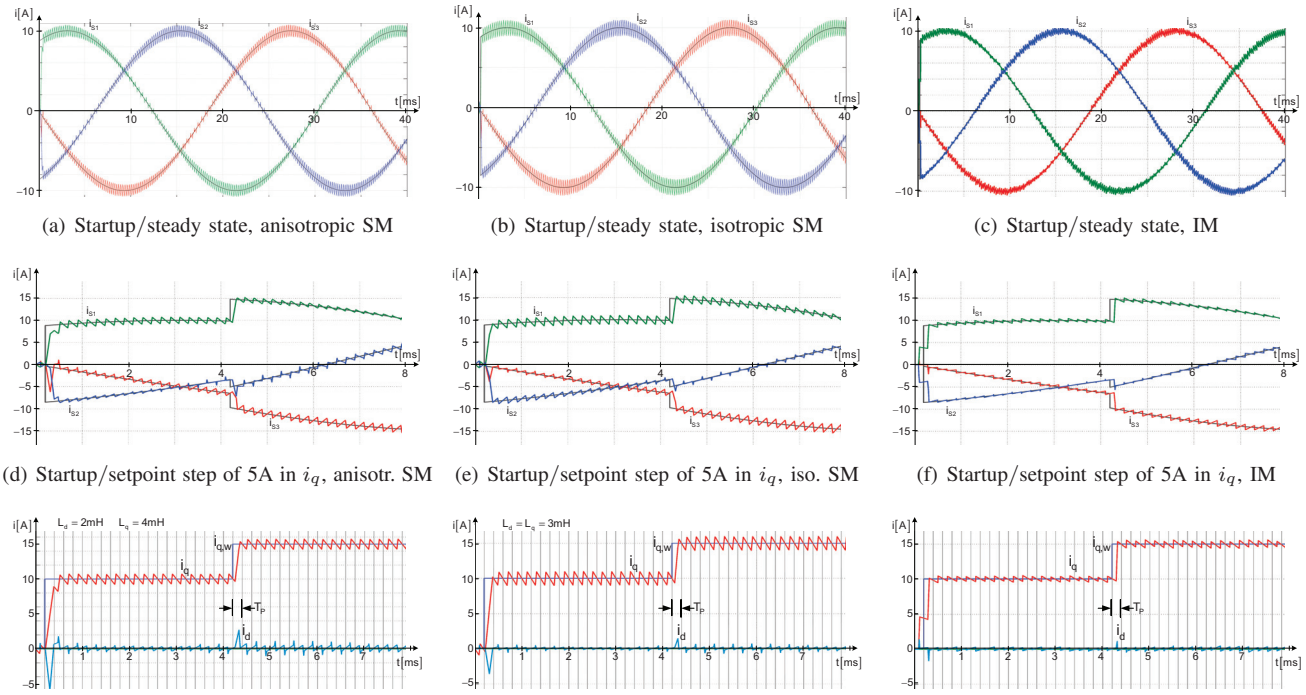

(a) Startup/steady state, anisotropic SM (b) Startup/steady state, isotropic SM (c) Startup/steady state, IM

(d) Startup/setpoint step of 5A in i_q, anisotr. SM (e) Startup/setpoint step of 5A in i_q, iso. SM (f) Startup/setpoint step of 5A in i_q, IM

(g) Startup/setpoint step of 5A in i_q, rotor oriented reference frame, anisotropic SM (h) Startup and setpoint step of 5A in i_q, rotor oriented reference frame, isotropic SM (i) Startup and setpoint step of 5A in i_q, flux oriented reference frame, IM

Figure 7. Simulation of startup, steady state operation and setpoint step response with the DACC control scheme for a magnetic anisotropic synchronous machine (SM) with L_d=2mH and L_q=4mH (Figures 7(a), 7(d)), 7(g)), a magnetic isotropic permanent magnet synchronous machine (SM) with $L_d = L_q$ = 3mH (Figures 7(b), 7(e)), 7(h)) and an induction machine (IM) (Figures 7(c), 7(f)), 7(i)) at $n = 400min^{-1}$, p=4 , f_p=5kHz, $i_{d,w}$=0A.

REFERENCES

[1] P. Cortes, M. Kazmierkowski, R. Kennel, D. Quevedo, and J. Rodriguez, "Predictive control in power electronics and drives," *Industrial Electronics, IEEE Transactions on*, vol. 55, no. 12, pp. 4312 –4324, dec. 2008.

[2] A. Linder and R. Kennel, "Model predictive control for electrical drives," in *Power Electronics Specialists Conference, 2005. PESC '05. IEEE 36th*, june 2005, pp. 1793 –1799.

[3] T. Gemassmer, J. Richter, M. Schnarrenberger, and M. Braun, "High dynamic rotor oriented current control for permanent magnet synchronous machines with saturation characteristics," in *PCIM Europe 2014, Nuremberg, Germany*, 2014.

[4] J. Richter, T. Gemassmer, and M. Doppelbauer, "Predictive current control of saturated cross-coupled permanent magnet synchronous machines," in *SPEEDAM 2014, Ischia (Italy), June 2014*, 2014.

[5] M. Schrödl, "Sensorless control of ac machines at low speed and standstill based on the inform-method," in *Industry Applications Conference, 1996. Thirty-First IAS Annual Meeting, IAS '96., Conference Record of the 1996 IEEE*, vol. 1, oct 1996, pp. 270 –277 vol.1.

[6] P. Landsmann, C. Hackl, and R. Kennel, "Eliminating all machine parameters in encoderless predictive torque control without signal injection," in *Electric Machines Drives Conference (IEMDC), 2011 IEEE International*, may 2011, pp. 1259 –1264.

[7] M. Schrödl and C. Simetzberger, "Sensorless control of pm synchronous motors using a predictive current controller with integrated inform and emf evaluation," in *Power Electronics and Motion Control Conference, 2008. EPE-PEMC 2008. 13th*, sept. 2008, pp. 2275 –2282.

[8] J. Weigold and M. Braun, "Predictive current control using identification of current ripple," *IEEE Transactions on Industrial Electronics*, vol. 55, no. 2, pp. 4346–4353, 2008.

[9] F. Becker, H. Ennadifi, and M. Braun, "Straightforward current control - one step controller based on current slope detection," in *EPE ECCE-EUROPE 2011 Birmingham*, 2011.

[10] F. Becker, "Ein neues adaptives verfahren zur hochdynamischen stromregelung," Ph.D. dissertation, Elektrotechnisches Institut, Karlsruher Institut für Technologie (KIT), 2011.

[11] A. Liske, P. Hofmeier, and M. Braun, "Extended straightforward current control for permanent magnet synchronous machines," in *Power Electronics and Applications (EPE), 2013 15th European Conference on*, 2013, pp. 1–10.

[12] H. Späth, *Elektrische Maschinen - Eine Einführung in die Theorie des Betriebsverhaltens*. Springer-Verlag, 1973.

[13] F. Becker, H. Ennadifi, and M. Braun, "Straightforward current control - one step controller based on current slope detection," *EPE Journal Volume 22-2*, 2012.

Andreas Liske received the Dipl.-Ing. degree in electrical engineering from the Karlsruhe Institute of Technology (KIT), Germany in 2010. Since 2010 he has been working as a research engineer at the Elektrotechnisches Institut (ETI), located at the Karlsruhe Institute of Technology (KIT), Germany to receive a PhD. His research interests are power electronics, modeling and adaptive control strategies.

Michael Braun received the Dipl.-Ing. and Dr.-Ing. degrees from the Technische Hochschule Darmstadt, Germany, in 1978 and 1983, respectively. From 1983 to 1994, he was with Siemens AG, Erlangen, Germany, where he was engaged in the development of power electronics and electrical drives. Since 1994, he has been a Professor and the Head of the Elektrotechnisches Institut (ETI), located at the Karlsruhe Institute of Technology (KIT), Germany. His research interests include power electronics, control of electrical drives, and mechatronics.